J Biomol NMR (2013) 55:59–70
DOI 10.1007/s10858-012-9686-6

ARTICLE

Influence of the O-phosphorylation of serine, threonine and tyrosine in proteins on the amidic ^{15}N chemical shielding anisotropy tensors

Jiří Emmer · Andrea Vavrinská · Vladimír Sychrovský · Ladislav Benda · Zdeněk Kříž · Jaroslav Koča · Rolf Boelens · Vladimír Sklenář · Lukáš Trantírek

Received: 16 August 2012 / Accepted: 15 November 2012 / Published online: 1 December 2012

Abstract Density functional theory was employed to study the influence of O-phosphorylation of serine, threonine, and tyrosine on the amidic ^{15}N chemical shielding anisotropy (CSA) tensor in the context of the complex chemical environments of protein structures. Our results indicate that the amidic ^{15}N CSA tensor has sensitive responses to the introduction of the phosphate group and the phosphorylation-promoted rearrangement of solvent molecules and hydrogen bonding networks in the vicinity of the phosphorylated site. Yet, the calculated ^{15}N CSA tensors in phosphorylated model peptides were in range of values experimentally observed for non-phosphorylated proteins. The extent of the phosphorylation induced changes suggests that the amidic ^{15}N CSA tensor in phosphorylated proteins could be reasonably well approximated with averaged CSA tensor values experimentally determined for non-phosphorylated amino acids in practical NMR applications, where chemical surrounding of the phosphorylated site is not known a priori in majority of cases. Our calculations provide estimates of relative errors to be associated with the averaged CSA tensor values in interpretations of NMR data from phosphorylated proteins.

Keywords CSA · Phosphorylation · Amidic nitrogen · Serine · Threonine · Tyrosine · Protein · NMR

Electronic supplementary material The online version of this article (doi:10.1007/s10858-012-9686-6) contains supplementary material, which is available to authorized users.

J. Emmer
Biology Centre, Academy of Science of the Czech Republic and University of South Bohemia, Branišovská 31, 370 05 České Budějovice, Czech Republic

A. Vavrinská · R. Boelens · L. Trantírek (✉)
Bijvoet Centre for Biomolecular Research, Utrecht University, 3584 CH Utrecht, The Netherlands
e-mail: l.trantirek@uu.nl

V. Sychrovský · L. Benda
Institute of Organic Chemistry and Biochemistry v.v.i., Academy of Science of the Czech Republic, Flemingovo nám. 2, 166 10 Prague, Czech Republic

Z. Kříž · J. Koča · V. Sklenář · L. Trantírek
National Centre for Biomolecular Research and CEITEC, Masaryk University, Kamenice 5, 602 00 Brno, Czech Republic

Introduction

The chemical shielding (CS) tensor of amidic nitrogen plays an increasingly important role in NMR analysis of protein structure. Perturbations in amide isotropic CS are often used to map protein–ligand interactions (Zuiderweg 2002) and to characterize the secondary structure of proteins (Cornilescu et al. 1999; Neal et al. 2006; Shen and Bax 2007; Shen et al. 2009). Anisotropy of the chemical shielding (CSA) tensor of amidic nitrogen is used to characterize the relative orientations of segments of membrane proteins with respect to the membrane (Mason et al. 2004), to characterize the secondary structure of proteins (Elavarasi and Dorai 2010), and as orientational restraints in the refinement of protein structures (Lipsitz and Tjandra 2003). Quantitative analysis of ^{15}N relaxation rates, which depend on the ^{15}N CSA, is widely used for the characterization of protein dynamics (Lipari and Szabo 1982a, b; Dellwo and Wand 1989; Kay et al. 1989; Peng and Wagner 1992; Fushman and Cowburn 2001). In addition, the interference between ^{15}N CSA and ^{1}H-^{15}N dipolar relaxation mechanisms form the basis for the TROSY experiment, a broadly used technique used to increase the resolution of large proteins and protein complexes (Pervushin et al. 1997).

Because of their importance, the ^{15}N CS tensors in amino acids, peptides, and proteins were subject of numerous experimental (Hiyama et al. 1988; Lumsden et al. 1993; Fushman and Cowburn 1998; Fushman et al. 1998; Lee et al. 1998; Kroenke et al. 1999; Boyd and Redfield 1999; Cornilescu and Bax 2000; Lee et al. 2001; Kurita et al. 2003; Waddell et al. 2005; Damberg et al. 2005; Lancelot et al. 2005; Burton and Tjandra 2006; Hall and Fushman 2006; Wylie et al. 2005, 2006, 2007; Yao et al. 2010; Pandey et al. 2012) and theoretical (De Dios et al. 1993; Le and Oldfield 1996; Brender et al. 2001; Xu and Case 2002; Poon et al. 2004; Bouř et al. 2005; Tang and Case 2007, 2011; Cai et al. 2008, 2009; Sychrovský et al. 2008; Benda et al. 2009; Saitôa et al. 2010) studies. The collective experimental findings have revealed the considerable site-specific variability of the ^{15}N CS tensors in proteins. Previous theoretical works provided explanation for the observed ^{15}N CS tensor variability by showing that the ^{15}N CS is dependent in a complex manner on the ϕ, ψ, and χ_1 backbone torsion angles, identity and conformation of the adjoining amino acids; hydrogen bonding partners of the amidic nitrogen; long-range electrostatic interactions; and solvent effects. Accounting for the site-specific differences in the ^{15}N CSA was demonstrated to be essential for physically meaningful analysis of structural and relaxation NMR data (Fushman and Cowburn 1999; Yao et al. 2010).

O-phosphorylation is the primary form of covalent modification for the regulation of proteins. It is estimated that at least 30–60 % of the proteins encoded by genes are subjected to phosphorylation, and the overwhelming majority of these proteins are phosphorylated at multiple sites (Hubbard and Cohen 1993; Cohen 2000; Pawson and Scott 2005; Jiménez et al. 2007). In most cells, approximately 90 % of protein phosphorylation occurs on serine, more than 9 % on threonine and $\sim$0.05 % on tyrosine residues (Pawson and Scott 2005; Jiménez et al. 2007). Since the phosphorylation-mediated regulation of protein activity is typically interconnected with functional protein dynamics, the ^{15}N NMR relaxation represents a suitable and obvious tool for investigation of molecular mechanisms of phosphorylation induced activation/deactivation of protein function (Volkman et al., 2001; Baker et al. 2007; Gardino et al. 2009; Otten et al. 2010).

Despite the importance of O-phosphorylation in protein biology, there has been no information on the amidic ^{15}N CSA tensor for O-phosphorylated amino acids. For NMR analysis of structure and dynamics of O-phosphorylated proteins using methods requiring information on amidic ^{15}N CSA tensor, a basic question remains to be answered, namely, the extent to which the amidic ^{15}N CSA tensor is affected by O-phosphorylation.

To aid in addressing this question, the effects caused by the O-phosphorylation of serine, tyrosine, and threonine

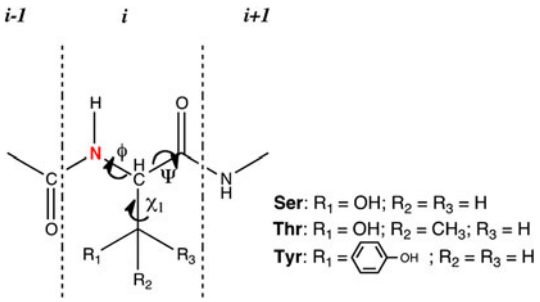

Fig. 1 Schematic representation of the serine (Ser), tyrosine (Tyr), and threonine (Thr). The amidic nitrogen is highlighted in *red*. In the O-phosphorylated Ser, Tyr, and Thr, the –OH moiety of R_1 is replaced by $-O-PO_3^{2-}$. The Ψ, ϕ, and χ_1 torsion angles are defined in accordance with IUPAC nomenclature (Markley et al. 1998)

(Fig. 1), the three most frequently phosphorylated amino acids in eukaryotic proteins, on the amidic ^{15}N CSA tensor were modeled using density functional theory (DFT) calculations. Taking into account that the O-phosphorylation of amino acids in proteins might be connected with conformational changes in the backbone, torsion angles of side-chains, and/or complex re-arrangements of the solvation layer accompanied with alterations in the hydrogen-bonding network and ion coordination, calculations for complex model systems were performed in respect to the native context of the structure of the protein.

Materials and methods

Analysis of crystallographic data and model selection

The PDB database (Berman et al. 2000) was used to identify protein crystal structures containing phosphorylated serine, threonine, or tyrosine. Based on the list of protein structures identified, the corresponding non-phosphorylated analogs were retrieved from the database as well. Selected pairs of the phosphorylated and non-phosphorylated structures were subsequently manually inspected. Only structures without perturbations from crystallization promoting precipitants (e.g., polyethylene glycol or heavy metal ions) and artificial contacts imposed by crystal packing within 10 Å surrounding the phosphorylated sites were considered for further analysis. After exclusion of duplicate structures, ten unique phosphorylated/non-phosphorylated protein pairs were obtained. The resolution, R-factors and PDB accession codes of the selected protein pairs are listed in Table S1 (Supplementary Information).

The high-resolution crystal structures (*see above*) were used as a source of the atom coordinates for the phosphorylated and non-phosphorylated model peptides. The models used in the NMR calculations were based on the tripeptide segments containing complete $i-1$, i, and $i+1$

residues, where i denotes the phosphorylated residue. All non-covalent and hydrogen bonding interactions with surrounding molecules and/or protein residues found in the crystal structures (e.g., neighboring amino acids, ions, and water molecules from the first and second hydration shell) were included in the models. Unless stated otherwise, the model peptides were terminated by a methyl group, which replaced the C(O) or Cα carbon of the $i - 2$ and $i + 2$ residues, respectively. Because physiological pH is 7.35, the phosphate group was modeled with a −2 charge (i.e., $R–PO_4^{2-}$). All the models employed in our calculations are displayed in Figure S1, S2, and S3 (Supplementary Information).

Quantum chemical calculations

Prior to the NMR calculations, the hydrogen atoms were added to the model peptides derived from the protein crystal structures. The geometries of the model peptides were optimized in four successive steps. In the first step, only the geometries of hydrogen atoms were relaxed with the PM3 method to decrease the computation time required for the second optimization step. In the second step, the geometry of the hydrogen atoms were gradient-optimized using the DFT method with the B3LYP exchange correlation functional (Becke 1993) and the 6-31G** atomic basis set (Hehre et al. 1972; Hariharan and Pople 1973; Francl et al. 1982; Clark et al. 1983). In the third step, while all torsion angles between heavy atoms were fixed, the bond lengths and bond angles in the model structures were first pre-optimized by PM3 energy minimization, and finally gradient optimized using the DFT method at B3LYP/6-31G** level of theory. The CS tensors were calculated using the GIAO approach (Wolinski et al. 1990) with the B3LYP functional and the IGLO-III basis set (Kutzelnigg et al. 1990). The polarizable continuum model (PCM) (Cossi et al. 2002) of water solvent was used throughout the calculations. All the calculations were performed with the Gaussian 09, Revision A.02 (Frisch et al. 2009).

To test the dependence of the calculated of ^{15}N CS tensor on the basis set type and the number of gaussian atomic basis functions, a series of calculations for phosphorylated and non-phosphorylated serine analogues (Supplementary Information, Figure S6) were performed. The geometries of the analogues were optimized at the same level as the models used in this study. The test involved the IGLO-II/III (Kutzelnigg et al. 1990), Dunning's cc-pVnz (n = D, T, Q, and 5) (Dunning 1989; Woon and Dunning 1993), and Pople's 6-31G**, 6-31+G*, and 6-311++G** basis sets (Hehre et al. 1972; Hariharan and Pople 1973; Krishnan et al. 1980; McLean and Chandler 1980; Francl et al. 1982; Clark et al. 1983). The parameters for the basis sets were downloaded from the EMSL Basis Set Exchange web portal (Feller 1996; Schuchardt et al. 2007).

The CSA tensor

A second-rank CS tensor in the principal axis system was obtained from the NMR calculations. The CS tensor was decomposed into isotropic and anisotropic (herein referred to as CSA tensor) parts. A traceless CSA tensor in the principal axis system was described by two adjustable parameters according to Haerberlen notation (Harris et al. 2008): the magnitude ($\Delta\sigma = \sigma_{zz} - 1/2(\sigma_{xx} + \sigma_{yy})$) and the asymmetry ($\eta = 3(\sigma_{yy} - \sigma_{xx})/2\Delta\sigma$) of the CSA tensor, where each of the three principal components of the CSA tensor relates to the σ_{iso} as follows: $|\sigma_{zz} - \sigma_{iso}| \geq |\sigma_{xx} - \sigma_{iso}| \geq |\sigma_{yy} - \sigma_{iso}|$. The σ_{iso} is defined as $\sigma_{iso} = 1/3(\sigma_{xx} + \sigma_{yy} + \sigma_{zz})$. The term $\Delta\sigma_{N,N–H}$, defined as $\sum_{i=x}^{z} \sigma_{ii}^{N}((3\cos^2\theta_{ii} - 1)/2)$, was used to monitor concerted changes in both the magnitude and orientation of the CSA tensor. The σ_{ii}^{N} corresponds to the *ii-th* principal component of the CSA tensor of the amidic nitrogen, and the θ_{ii} is the projection angle between the $N–H^N$ bond and the σ_{ii}^{N}. Note that $\Delta\sigma_{N,N–H}$ corresponds to the effective term responsible for the modulation of the cross-correlated relaxation rates between the amidic ^{15}N CSA and $N–H^N$ dipole–dipole interaction. The θ_{ii} projection angles were also used to monitor the orientation of the CSA tensor in the molecular frame.

Results and discussion

Structural impact of O-phosphorylation

The selection criteria that were used as the PDB database was searched (see "Materials and methods") yielded ten unique phosphorylated/non-phosphorylated protein pairs (Supplementary Information—Table S1). Visual inspection of the differences between the non-phosphorylated and phosphorylated protein structures revealed that the O-phosphorylation generally had little effect on the backbone and side chain conformations of the phosphorylated residue itself and the backbone conformation of the adjoining amino acids (Table 1). These observations are in accordance with the general notion that O-phosphorylation of serine, threonine, and tyrosine in proteins is locally structurally silent (Johnson and Lewis 2001). In contrast to the minute impact of O-phosphorylation on the local structure, the reorganization of solvent molecules and the hydrogen bonding network in the vicinity of the phosphorylated site was determined to be dramatic in all investigated pairs (cf. Supplementary Information—Figure S1, S2, S4, and S5). These findings indicated that solvent

Table 1 Structural differences between the non-phosphorylated and phosphorylated (marked by subscript *P*) protein pairs employed in the NMR calculations

	Struct. class.[b]		$i-1$		i			$i+1$	
	1°	2°	$\lvert\Psi_P-\Psi\rvert$	$\lvert\phi_P-\phi\rvert$	$\lvert\Psi_P-\Psi\rvert$	$\lvert\phi_P-\phi\rvert$	$\lvert\chi_{1P}-\chi_1\rvert$	$\lvert\Psi_P-\Psi\rvert$	$\lvert\phi_P-\phi\rvert$
Pair[a]									
Serine									
I	K-**S**-I	C	1.2	2.6	7	4.3	6	14.4	7.3
II	G-**S**-N	C	4.6	6.4	1.2	0.2	8.5	4.1	0.7
III	S-**S**-E	H	1.3	3.3	0.1	3.4	1.4	4.3	1.2
IV	S-**S**-E	H	0.5	1.9	0.3	1.7	36.6	1.2	1.3
V	H-**S**-M	C	3	2.8	0.6	1.9	22.1	5.3	3.8
Pair[b]									
Tyrosine									
VI	E-**Y**-M	C	3.4	4.2	0.7	1.1	4.4	0.3	0.6
VII	S-**Y**-V	E	2.1	9.1	0.2	0.1	3.1	10.0	15.6
VIII	V-**Y**-A	E	0.3	1.5	0.8	3.6	0.7	15.2	4.4
IX	S-**Y**-V	E	1.1	7.3	2.9	0.7	1.7	2.3	3.0
Threonine									
X	K-**T**-L	C	12.1	0.9	11.6	31.1	10.8	3.6	39

The Ψ, ϕ, and χ_1 torsion angles are defined in accordance with IUPAC nomenclature (Markley et al. 1998). The differences are given in degrees

[a] I, II, III, IV, V, VI, VII, VIII, IX, and X correspond to the phosphorylated/non-phosphorylated pairs of proteins identified with the following PDB numbers: 2AK7/1MU4, 2FWN/1BFD, 2BZI/2BZH, 3CY3/3CXW, 3EXH/3EXE, 2QO7/2QO9, 2X2M/2IVS, 3CD3/3CBL, 3CI5/1NM1, and 3D5 W/3D5U

[b] The 1° (primary) structure is given in one-letter amino-acid codes. The 2° (secondary) structure is coded as follows: H, E, and C correspond to the α-helix, β-sheet, and random coil, respectively

reorganization due to phosphorylation might be one of the important factors that contributes to phosphorylation-induced perturbations of amidic ^{15}N CSA.

The calculation method and design of model peptides

The analysis of the selected crystal structures clearly indicated that the models to be employed for the calculation of the ^{15}N CS tensors in both the phosphorylated and non-phosphorylated proteins needed to reflect the intra-protein non-covalent interactions and the interactions between the protein and solvent molecules. However, these requirements have direct implications with respect to the size of the model peptides used in the NMR calculations. The sizes of the calculation model restricted the choice of the calculation method that was used.

It is known that the accuracy of calculated NMR parameters depends on the quality of the atomic basis set employed in the calculations (Helgaker et al. 1999; Xu and Case 2002). While predictions of the conformationally dependent changes of CS perform well for even relatively small basis sets (e.g., 6-31G**), the small basis sets are known to have deficiencies when used to compute the CS in different environments (Baldridge and Siegel 1999; Wang et al. 2001, 2002; Xu and Case 2002). In our case, the calculations of ^{15}N CS tensors for the amide nitrogen were performed in environments differing in solvent organization and in the presence/absence of the phosphate group using model systems that were fairly large (i.e., up to 150 atoms). Therefore, the choice of atomic basis set had to balance and compromise between the reliability of the calculated NMR data and the computational costs.

To select the basis set for calculation of the NMR parameters, dependence of the calculated ^{15}N CS tensor on the type of basis set and the number of gaussian atomic basis functions was evaluated. Serine and its phosphorylated analog were used as models for the analysis (Supplementary Information Figure S6). The effects of the atomic basis set on the calculated $\Delta\sigma$ and $\Delta\sigma_{N,N-H}$ values are summarized in Fig. 2.

While, independent of type of the basis set, the absolute values of calculated $\Delta\sigma$ were notably changing (increasing) along with increasing number of gaussian atomic basis functions in both non-phosphorylated and phosphorylated serine analogues (Fig. 2), the phosphorylation induced changes in $\Delta\sigma$, here referred to as $\Delta\Delta\sigma$, were virtually insensitive to basis set type and size. The $\Delta\Delta\sigma$ values calculated using all basis sets ranged from 1.08 to 3.38 ppm, with variance of 0.57 ppm (data not shown). Considering that $\Delta\Delta\sigma$ variability in complex model

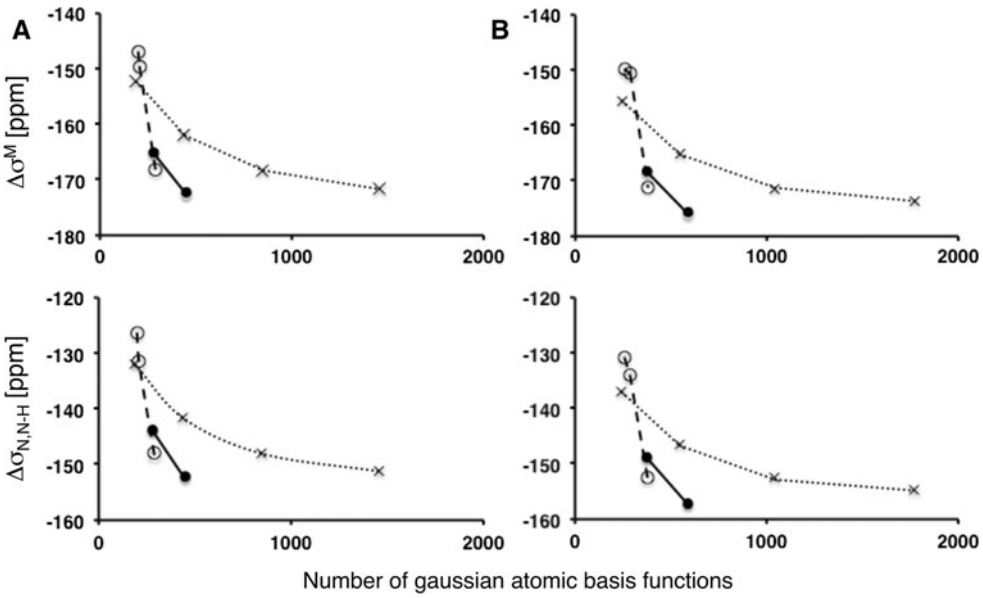

Fig. 2 $\Delta\sigma$ and $\Delta\sigma_{N,N-H}$ (in ppm) calculated for non-phosphorylated (**a**) and O-phosphorylated (**b**) serine analog (Supplementary Information—Figure S6) with the IGLO-II and IGLO-III (*filled circles—solid line*), Dunning's cc-pVnZ (n = D, T, Q, 5) (*crosses—dotted line*), and Pople's 6-31G**, 6-31+G*, and 6-311++G** (*open circles—dashed line*) basis sets

systems typically range between 5 to 9 ppm (cf. Tables 3, 4, 5), the variance of 0.57 ppm in $\Delta\Delta\sigma$ due to the basis set type and size can be regarded as small. As the IGLO-III basis set is known to be suited for calculations of NMR parameters (Jensen 2008), because its accuracy and low computational costs, we used this basis set for calculations of the phosphorylation-induced changes in $\Delta\sigma$ and $\Delta\sigma_{N,N-H}$ parameters of the amidic CS amidic tensor.

As originally suggested by Xu and Case (2002) and recently confirmed by Cai et al. (2009), the CS calculations for amino acids in α-helical segments should be performed using a 7–9 residue-long construct to suppress terminal artifacts. The terminal artifacts may include (1) a lack of hydrogen bonding partners for the considered residue from either ends or (2) an underestimation of the interaction of the residue with the dipole moment of the α-helix. To assess the minimal size of the structural models to be employed in the NMR calculations, reference calculations were performed with: (1) a basic model containing complete $i-1$, i, and $i+1$ residues and (2) an extended construct including full backbone and side chains of the $i \pm 3$, $i \pm 2$, and $i \pm 1$ amino acids adjoining the phosphorylation site i. Notably, although the sizes of the models, both basic and extended, were different, the models were constructed in a way that completely preserved all the protein–protein, protein-solvent, and solvent–solvent non-covalent interactions. Structural representations of the reference basic and extended models based on the crystal structure of phosphorylated human protein PIM1 (PDB ID: 2BZI) and the non-phosphorylated analog (PDB ID: 2BZH) that were used for the calculations are displayed in the Figure S7 (Supplementary Information). A comparison of the calculated CSA tensor parameters between the basic and extended models is given in Table 2.

Table 2 The magnitudes ($\Delta\sigma$), asymmetries (η), and orientations ($|\cos\theta_{ii}|$) of the amidic ^{15}N CSA tensors calculated using the basic and extended models derived from the *2BZI* (phosphorylated (+P)) and *2BZH* (non-phosphorylated (−P)) protein structures

Model	$\Delta\sigma$ (ppm)	η	$\lvert\cos\theta_{zz}\rvert$ (°)	$\lvert\cos\theta_{xx}\rvert$ (°)	$\lvert\cos\theta_{yy}\rvert$ (°)	$\Delta\sigma_{N,N-H}$ (ppm)
Basic						
−P	−163.16	0.30	0.95	0.08	0.30	−137.27
+P	−170.26	0.17	0.92	0.23	0.31	−131.12
Extended						
−P	−163.20	0.29	0.95	0.08	0.30	−136.98
+P	−170.44	0.17	0.92	0.24	0.31	−131.26

The calculations were performed including explicitly coordinated solvent molecules. The structural representations of the basic and extended models are shown in Supplementary Information Figure S7. For specific details on the calculations see Supplementary Information Figure S7

As shown in Table 2, the $\Delta\sigma$ and $\Delta\sigma_{N,N-H}$ values calculated using the basic and extended models are very similar for both the phosphorylated and non-phosphorylated structures. While results by Cai et al. (2009) indicated that up to a 6.6 ppm difference could be obtained due to helical dipole moments between models based on i_{-1}-*to*-i and i_{-4}-to-i_{+3} peptides, the calculations in this report revealed only less than 0.5 ppm (<2 ‰) difference between the amidic CSA tensor magnitudes calculated for the basic (i_{-1}-to-i_{+1}) and extended (i_{-3}-to-i_{+3}) models. This comparison indicates that in our case the basic model already included the most important interactions required for an adequate description of the chemical environment of the amidic nitrogen. All the NMR calculations in this study were thus performed using the basic models.

The protein-solvent interactions

As already mentioned, within the investigated data set, O-phosphorylation had very little effect on the local structure surrounding the phosphorylated site (Table 1). However, the analysis of the crystal structures revealed that phosphorylation was associated with the reorganization of solvent molecules and the hydrogen-bonding network in the vicinity of a phosphorylated site. To estimate the effects caused by site-specifically coordinated solvent molecules on both the $\Delta\sigma$ and $\Delta\sigma_{N,N-H}$, the calculated CSA tensors were compared, where the explicit solvent molecules were fully preserved and where the explicit solvent molecules were removed and the solvent effects were simulated only with the implicit PCM of water solvent. The amidic CSA tensors for non-phosphorylated and phosphorylated protein models calculated with explicit solvent molecules and the implicit solvent model are given in Tables 3, 4 and Tables S2, S3 (Supplementary information), respectively. Within the phosphorylated data set, the calculated differences for the $\Delta\sigma$ and $\Delta\sigma_{N,N-H}$ between the corresponding models that employed explicit and implicit solvent ranged from 0.3 to 13.1 ppm and from 0.4 to 22.3 ppm, respectively. Within the non-phosphorylated data set, the corresponding differences were between 0.6 and 13.9 ppm and between 0.8 and 28.9 ppm, respectively. Poor mutual correlation of both the $\Delta\sigma$ and $\Delta\sigma_{N,N-H}$ values calculated using the two solvent models indicated that inclusion of the explicit solvation in CSA tensor calculations was necessary for both the non-phosphorylated and phosphorylated peptides. The correlation determined for $\Delta\sigma_{N,N-H}$ was notably worse than the correlation for $\Delta\sigma$. This result agrees with the observed notable impact of the solvent model on the asymmetries and orientations of the CSA tensor (cf. Tables 3, 4 and Table S2 and S3).

Impact of O-phosphorylation on amidic ^{15}N CSA: serine

Searching the PDB database yielded five unique pairs of proteins with non-phosphorylated and phosphorylated serine residues (Supplementary Information—Table S1). The calculated CSA tensors in the serine residues for both the non-phosphorylated and phosphorylated protein pairs are reported in Table 3. As can be observed, notable changes in magnitude, asymmetry, and orientation of the CSA tensors were calculated upon phosphorylation. The phosphorylation-induced changes in the $\Delta\sigma$ were generally less than 9 ppm and did not exceed 14.6 ppm. The phosphorylation-induced changes in $\Delta\sigma_{N,N-H}$, a term that reflects both the CSA tensor magnitude and orientation, were approximately 10 ppm on average and did not exceed 19.3 ppm.

In terms of the identity of the residues adjoining the phosphorylated site, solvation patterns, local backbone conformations, and side-chain conformations, the set of the non-phosphorylated and phosphorylated proteins used in the calculations was highly diverse (Table 1, Supplementary Information Figure S1). Despite the notable diversity in the chemical environment, the pair-wise differences among the CSA tensor magnitudes within the investigated data sets for the phosphorylated and non-phosphorylated serines were moderate: 6.8 and 8.2 ppm on average, respectively (Table 3). The maximal differences among the individual $\Delta\sigma$ values did not exceed 16.1 ppm in both data sets. Figure 3 shows a comparison of the ranges of the $\Delta\sigma$ and $\Delta\sigma_{N,N-H}$ values calculated separately for the phosphorylated

Table 3 The magnitudes ($\Delta\sigma$), asymmetries (η), and orientations ($|\cos\theta_{ii}|$) of the amidic ^{15}N CSA tensors calculated for the model structures with non-phosphorylated (−P) and phosphorylated (+P) serine residues

Pairs I, II, III, IV, and V correspond to the phosphorylated/non-phosphorylated pairs of proteins identified with the following PDB numbers: 2AK7/1MU4, 2FWN/1BFD, 2BZI/2BZH, 3CY3/3CXW, and 3EXH/3EXE

Pair no.	$\Delta\sigma$ (ppm)	η	$\lvert\cos\theta_{zz}\rvert$ (°)	$\lvert\cos\theta_{xx}\rvert$ (°)	$\lvert\cos\theta_{yy}\rvert$ (°)	$\Delta\sigma_{N,N-H}$ (ppm)
I						
+P	−175.42	0.08	0.96	0.16	0.25	−152.45
−P	−184.41	0.07	0.95	0.09	0.31	−155.77
II						
+P	−174.75	0.21	0.95	0.02	0.31	−147.91
−P	−180.57	0.32	0.96	0.05	0.27	−157.34
III						
+P	−177.14	0.19	0.92	0.20	0.34	−134.60
−P	−171.53	0.22	0.94	0.11	0.32	−140.05
IV						
+P	−182.86	0.16	0.95	0.03	0.30	−155.90
−P	−168.34	0.38	0.94	0.23	0.27	−136.62
V						
+P	−167.13	0.12	0.90	0.34	0.27	−119.92
−P	−176.05	0.18	0.92	0.15	0.37	−132.97

and non-phosphorylated model peptides. As can be observed in both the phosphorylated and non-phosphorylated model peptides, the $\Delta\sigma$ values for the amidic nitrogens spanned virtually identical regions. In terms of practical applications, the calculations indicate that the $\Delta\sigma$ in both the phosphorylated and non-phosphorylated serines can in principle be approximated with single, phosphorylation-state unspecific CSA tensor magnitude. Pair-wise differences among the CSA tensor magnitudes within the investigated data sets for the non-phosphorylated and phosphorylated serines resulted in an estimate for the relative error ($\pm$ 4.3 %) to be associated with the phosphorylation-state unspecific $\Delta\sigma$ (-175.8 ppm) (Table 3). The calculated values agree reasonably well with recently reported amino-acid type unspecific $\Delta\sigma$ values by Yao et al. (2010) in α-helical and β-sheet protein segments, which were -173 ppm $\pm$ 4.1 % and -162 ppm $\pm$ 3.7 %, respectively. Notably, the data set in this report comprises of protein pairs that contain α-helical and random coil protein segments (Table 1).

The phosphorylation-induced changes in the $\Delta\sigma_{N,N-H}$, the term responsible for modulation of the cross-correlated relaxation rates between the N–H dipole–dipole and amidic nitrogen CSA, were 10.1 ppm on average and did not exceed 19.3 ppm (Table 3). Although these changes were comparable to the phosphorylation-induced changes in the $\Delta\sigma$, the comparison of the calculated $\Delta\sigma_{N,N-H}$ values within the non-phosphorylated and phosphorylated data sets revealed significantly higher pair-wise differences among the $\Delta\sigma_{N,N-H}$ values compared to the differences observed for the $\Delta\sigma$ values. While the calculated pair-wise differences among $\Delta\sigma_{N,N-H}$ values calculated for phosphorylated serines were $\sim$18.0 ppm on average with a maximal observed difference of $\sim$36.0 ppm, the pair-wise differences among the $\Delta\sigma_{N,N-H}$ values for non-phosphorylated serines were 13.6 ppm on average with a maximal difference of $\sim$24.4 ppm. The calculated $\Delta\sigma_{N,N-H}$ values (Table 3) indicate that while the single, phosphorylation-state unspecific $\Delta\sigma_{N,N-H}$ value (-143.4 ppm) could still be used for the interpretation of the corresponding cross-correlated relaxation rates in both the phosphorylated and non-phosphorylated serines, the distinct associated relative errors of at least $\pm$ 9.5 and $\pm$ 12.6 % should be used for non-phosphorylated and phosphorylated serines, respectively, to account for the chemical environment-dependent variability in $\Delta\sigma_{N,N-H}$.

The impact of O-phosphorylation on amidic ^{15}N CSA: tyrosine

Searching the PDB database, while applying the stringent selection criteria (see "Materials and methods"), yielded four unique pairs of proteins with non-phosphorylated and phosphorylated tyrosine residues (Supplementary Information—Table S1). The amidic nitrogen CSA tensors calculated for the tyrosine residues in the selected non-phosphorylated and phosphorylated protein pairs are reported in Table 4. Similar to the situation in the phosphorylated serines, the O-phosphorylation of tyrosine produced notable changes in the magnitude, shape and orientation of the CSA tensor. Within the investigated data set, the phosphorylation-induced changes in $\Delta\sigma$ were 8.0 ppm on average, and did not exceed 16.0 ppm. For $\Delta\sigma_{N,N-H}$, the phosphorylation-induced changes were 8.3 ppm on average, and did not exceed 10.7 ppm.

The calculated pair-wise difference for the $\Delta\sigma$ values among the phosphorylated and non-phosphorylated structures was 13.2 ppm and 10.5 ppm on average, respectively.

Table 4 The magnitudes ($\Delta\sigma$), asymmetries (η), and orientations ($|\cos\theta_{ii}|$) of the amidic ^{15}N CSA tensors calculated for the model structures with non-phosphorylated ($-$P) and phosphorylated (+P) tyrosine residues

Pair no.	$\Delta\sigma$ (ppm)	η	$\lvert\cos\theta_{zz}\rvert$ (°)	$\lvert\cos\theta_{xx}\rvert$ (°)	$\lvert\cos\theta_{yy}\rvert$ (°)	$\Delta\sigma_{N,N-H}$ (ppm)
VI						
+P	-188.38	0.35	0.96	0.05	0.26	-166.14
$-$P	-187.11	0.39	0.95	0.07	0.31	-155.49
VII						
+P	-172.87	0.31	0.96	0.00	0.28	-150.54
$-$P	-180.96	0.20	0.96	0.06	0.29	-156.49
VIII						
+P	-173.58	0.22	0.96	0.09	0.25	-154.01
$-$P	-167.07	0.29	0.96	0.09	0.26	-147.41
IX						
+P	-162.28	0.13	0.95	0.09	0.31	-135.61
$-$P	-178.26	0.08	0.94	0.08	0.34	-145.72

Pairs VI, VII, VIII, and IX correspond to the phosphorylated/non-phosphorylated pairs of proteins identified with the following PDB numbers: 2QO7/2QO9, 2X2M/2IVS, 3CD3/3CBL, and 3CI5/1NM1

The respective pair-wise differences for $\Delta\sigma_{N,N-H}$ were 15.8 and 6.7 ppm on average. Figure 3 shows ranges for $\Delta\sigma$ and $\Delta\sigma_{N,N-H}$ values calculated separately for the non-phosphorylated and phosphorylated tyrosine residues in selected model structures. Again, in the non-phosphorylated and phosphorylated tyrosine pairs, the calculated $\Delta\sigma$ and $\Delta\sigma_{N,N-H}$ values spanned similar regions. Notably, for the $\Delta\sigma_{N,N-H}$, the calculated pair-wise differences in non-phosphorylated structures were appreciably smaller than the differences for the phosphorylated tyrosines.

Similar to the situation for the serine residues, the calculations indicate that the amidic CSA tensor for both the non-phosphorylated and O-phosphorylated tyrosine residues could be approximated using the phosphorylation-state unspecific $\Delta\sigma$ and $\Delta\sigma_{N,N-H}$ values of −176.3 and −151.4 ppm, respectively (Table 4). For non-phosphorylated tyrosine residues, the estimates of associated minimal relative errors are ± 6.0 and ± 4.4 %, respectively. For phosphorylated tyrosine residues, the calculations suggest that the associated relative errors should be set to at least to ± 7.5 and ± 10.4 %, respectively.

Impact of O-phosphorylation on amidic ^{15}N CSA: threonine

Only one unique pair of non-phosphorylated and phosphorylated analogues passed the stringent criteria applied to the PDB search (Supplementary Information—Table S1). The calculated CSA tensors of the amidic nitrogen in the threonine residues for the selected non-phosphorylated and phosphorylated protein pair are reported in Table 5 and shown in Fig. 3. In the investigated pair, the phosphorylation-induced changes in $\Delta\sigma$ and $\Delta\sigma_{N,N-H}$ were 27.51 and 19.34 ppm, respectively.

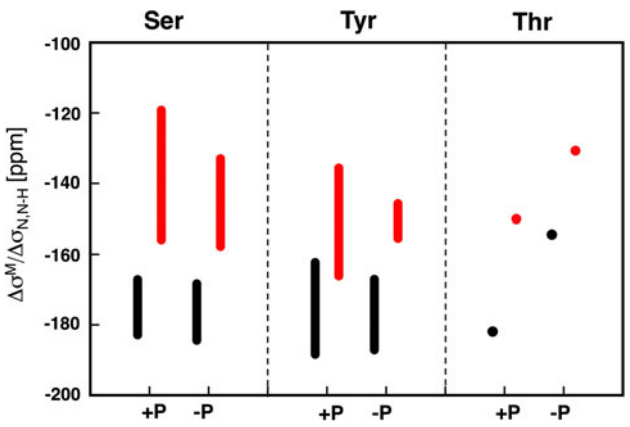

Fig. 3 Comparison of the ranges of the calculated $\Delta\sigma$ (*black bar*) and $\Delta\sigma_{N,N-H}$ (*red bar*) values in selected non-phosphorylated (−P) and O-phosphorylated (+P) proteins. The ranges are defined by the calculated minimum and maximum values for $\Delta\sigma$ and $\Delta\sigma_{N,N-H}$ in Tables 3, 4 and 5

Comparison of calculated amidic CSA tensor with experiment

To assess the applicability of the calculations, the calculated $\Delta\sigma$ values for the non-phosphorylated residues in our model structures were compared with experimental data available in the literature (Damberg et al. 2005; Wylie et al. 2006; Hall and Fushman 2006; Yao et al. 2010). The comparison revealed that the $\Delta\sigma$ values calculated for the non-phosphorylated serines, threonines, and tyrosines were well in the ranges for the $\Delta\sigma$ values experimentally observed for non-phosphorylated residues in proteins (Fig. 4). In addition, the calculated θ angles between the least shielded CSA tensor component and N–H^N bond in the non-phosphorylated amino acids, being on average 19.1 ± 1° (cf. the $|\cos\theta_{zz}|$ values in Tables 3, 4, and 5), were in good agreement with experimental data, which

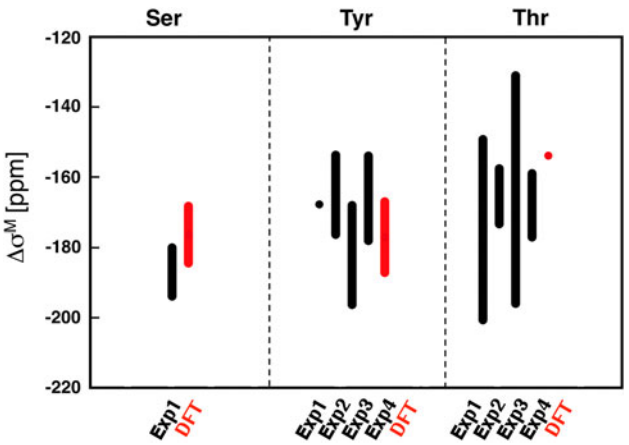

Fig. 4 Comparison of experimental (*black bar*) and calculated (*red bar*) minimum and maximum $\Delta\sigma$ values in non-phosphorylated proteins. The $\Delta\sigma$ values denoted here as Exp1, Exp2, Exp3, and Exp4 were extracted from the references Damberg et al. (2005), Wylie et al. (2006), Hall and Fushman (2006), and Yao et al. (2010), respectively

Table 5 The magnitudes ($\Delta\sigma$), asymmetries (η), and orientations ($|\cos\theta_{ii}|$) of the amidic ^{15}N CSA tensors calculated for the model structures with non-phosphorylated (−P) and phosphorylated (+P) threonine residues

Pair no.	$\Delta\sigma$ (ppm)	η	$\lvert\cos\theta_{zz}\rvert$ (°)	$\lvert\cos\theta_{xx}\rvert$ (°)	$\lvert\cos\theta_{yy}\rvert$ (°)	$\Delta\sigma_{N,N-H}$ (ppm)
X						
+P	−181.91	0.13	0.94	0.13	0.31	−150.05
−P	−154.40	0.19	0.95	0.24	0.22	−130.71

The calculations were performed with the use of the implicit solvent model (PCM) only as in corresponding crystal structures no explicit solvent molecules could be identified in vicinity of the phosphorylated residue

Pair X corresponds to the phosphorylated/non-phosphorylated pair of proteins identified with the PDB number: 3D5 W/3D5U

indicated that the range was 19.6 ± 2.5° (Yao et al. 2010). Altogether, the agreement between experimental and calculated CSA tensors obtained for non-phosphorylated amino acids provides justification for the appropriateness of the choice of computational models and a choice of the basis set employed in the calculations.

Influence of the phosphate group charge on amidic CSA tensor

It should be mentioned that our calculations describe somewhat extreme situation of the constant fixed charge of -II, which is expected for a phosphate group at physiological pH. Nonetheless, in buffered solutions as well as in intracellular environment, the highly charged phosphate group is expected to interact with counter ions and water molecules. These interactions can diminish the effective charge of the phosphate group. To find out how phosphate group charge influences amidic ^{15}N CSA, we remodeled PO_4^{2-} group into HPO_4^{-} in three model structures, namely 2FWN (serine), 2X2M (tyrosine), and 3D5 W (threonine). To decrease effective charge at phosphate group, we employed concept of phosphate-protonation as it corresponds to physiologically relevant process.

In all model cases, the protonation-mediated reduction of phosphate group effective charge resulted in decrease of the absolute value of the amidic ^{15}N CSA magnitude (Supplementary Information—Table S5). In absolute numbers, the decrease ranged between 0.6 and 4.1 ppm. In the 2FWN/1BFD protein pair, the HPO_4^{-} induced change in the amidic ^{15}N CSA magnitude was for 3.25 ppm larger than that induced by PO_4^{2-} group. Also for the 2X2M/2IVS pair, the HPO_4^{-} group induced bigger change (for 0.63 ppm) than the PO_4^{2-} group. However, for the 3D5 W/3D5U pair, the HPO_4^{-} induced change in amidic ^{15}N CSA magnitude was smaller for 4.2 ppm compared to that induced by the PO_4^{2-} group. These calculations indicate that reduction of the phosphate group charge might result either in increase or decrease in amidic ^{15}N CSA magnitude depending on attributes of the chemical environment in vicinity of the phosphorylated site.

Conclusions

In this study, the impact of O-phosphorylation on the CSA tensor of the amidic nitrogen in serine, threonine, and tyrosine was estimated using the DFT calculations. The results indicate that the amidic CSA tensor sensitively responds to both the introduction of the phosphate group and the phosphorylation-promoted rearrangement of solvent molecules and the hydrogen-bonding network in the vicinity of the phosphorylated site. The extent of changes in the amidic nitrogen CSA tensor due to introduction of the phosphate group appears to depend on both local structure at the phosphorylated site and identity of adjoining amino acids. Unfortunately, in practical NMR applications requiring information on amidic ^{15}N CSA tensor of phosphorylated amino acid, the dependence of amidic ^{15}N CSA tensor on primary, secondary and tertiary structure cannot be exploited for interpretation of NMR data as ever-present contribution from solvation and hydrogen-bonding at the phosphorylated site is not usually known a priori and it cannot be easily estimated. Notably, the calculated ^{15}N CSA tensor magnitudes and orientations in phosphorylated and solvated model peptides were in range of values experimentally observed for non-phosphorylated proteins. This suggests that the amidic ^{15}N CSA tensor in phosphorylated proteins could be reasonably well approximated with averaged CSA tensor values experimentally determined for non-phosphorylated amino acids (Yao et al. 2010) in practical NMR applications, where chemical surrounding of the phosphorylated site is not known a priori. In the same time, our calculations indicated somewhat larger chemical environment-dependent variability of the $\Delta\sigma_{N,N-H}$ values in phosphorylated compared to non-phosphorylated proteins. Our calculations provide estimates of relative errors to be associated with the averaged CSA tensor values in interpretations of NMR data from phosphorylated proteins.

A word of caution: The DFT calculations only provided static CSA values, which accounted for neither the dynamical phenomena (e.g., vibrational averaging) at investigated sites (Tang and Case 2007) nor the dynamics of solvent molecules. Nonetheless, the comparative analysis of crystallographic B-factors among the phosphorylated and non-phosphorylated proteins (data not shown) indicates that the mobility of backbone of the investigated proteins was similar, which implies that a similar level of dynamical averaging of the nitrogen CSA in both the phosphorylated and non-phosphorylated residues should occur. Whereas the phosphorylation induced changes in σ_{iso} measured for inherently highly dynamic disordered proteins/protein regions typically range from 1 to 5 ppm (Metcalfe et al. 2005; Landrieu et al. 2006; Liokatis et al. 2010, 2012), the changes calculated here from static structures are notably higher ranging from 1.6 to 27.4 ppm. This comparison indicates that the notable differences in apparent CS(A) values might arise from dynamical phenomena and it supports the notion that the effective value of CS tensor can be used as a sensitive reporter of intramolecular dynamics. However, to properly evaluate the dynamics at phosphorylated residues, the CSA validated on well-defined structures such as those employed in our study needs to be known a priori.

Additionally, the size of the investigated data set was small due to the currently limited availability of high-quality crystallographic structures of mutually corresponding phosphorylated and non-phosphorylated protein pairs. However, considering the relatively high degree of diversity within the data set that was investigated in terms of identity of residues adjoining the phosphorylated sites, solvation patterns, local side-chain conformations, and backbone conformations, the present calculations appear to provide a reasonable estimate of the impact that the O-phosphorylation has on the amidic nitrogen CSA tensor.

Acknowledgments This work was supported by a VIDI career development grant by the Netherlands Organization for Scientific Research (NWO), by grant P205/10/0228 from Czech Science Foundation, and by the project "CEITEC—Central European Institute of Technology" (CZ.1.05/1.1.00/02.0068) from European Regional Development Fund. The access to computing and storage facilities owned by parties and projects contributing to the National Grid Infrastructure MetaCentrum, provided under the programme "Projects of Large Infrastructure for Research, Development, and Innovations" (LM2010005) is highly appreciated.

References

Baker JMR, Hudson RP, Kanelis V, Choy WY, Thibodeau PH, Thomas PJ, Forman-Kay JD (2007) CFTR regulatory region interacts with NBD1 predominantly via multiple transient helices. Nat Struct Mol Biol 14:738–745

Baldridge KK, Siegel JS (1999) Correlation of empirical delta (TMS) and absolute NMR chemical shifts predicted by ab initio computations. J Phys Chem A 103:4038–4042

Becke AD (1993) Density-functional thermochemistry. 3. The role of exact exchange. J Chem Phys 98:5648–5652

Benda L, Bouř P, Muller N, Sychrovský V (2009) Theoretical study of the effective Chemical Shielding Anisotropy (CSA) in peptide backbone, rating the impact of CSAs on the cross-correlated relaxations in L-alanyl-L-alanine. J Phys Chem B 113:5273–5281

Berman HM, Westbrook J, Feng Z, Gilliland G, Bhat TN, Weissig H, Shindyalov IN, Bourne PE (2000) The protein data bank. Nucl Acids Res 28:235–242

Bouř P, Buděšínský M, Špirko V, Kapitán J, Šebestík J, Sychrovský V (2005) A complete set of NMR chemical shifts and spin–spin coupling constants for L-Alanyl-L-alanine zwitterion and analysis of its conformational behavior. J Am Chem Soc 127:17079–17089

Boyd J, Redfield C (1999) Characterization of N-15 chemical shift anisotropy from orientation-dependent changes to N-15 chemical shifts in dilute bicelle solutions. J Am Chem Soc 121:7441–7442

Brender JR, Taylor DM, Ramamoorthy A (2001) Orientation of amide-nitrogen-15 chemical shift tensors in peptides: a Quantum Chemical Study. J Am Chem Soc 123:914–922

Burton RA, Tjandra N (2006) Determination of the residue-specific 15N CSA tensor principal components using multiple alignment media. J Biomol NMR 35:249–259

Cai L, Fushman D, Kosov DS (2008) Density functional calculations of 15N chemical shifts in solvated dipeptides. J Biomol NMR 41:77–88

Cai L, Fushman D, Kosov DS (2009) Density functional calculations of chemical shielding of backbone 15N in helical residues of protein G. J Biomol NMR 45:245–253

Clark T, Chandrasekhar J, Spitznagel GW, Schleyer PV (1983) Efficient diffuse function-augmented basis sets for anion calculations. III. The 3–21-+G basis set for first-row elements, Li-F. J Comput Chem 4:294–301

Cohen P (2000) The regulation of protein function by multisite phosphorylation—a 25 year update. Trends Biochem Sci 25:596–601

Cornilescu G, Bax A (2000) Measurement of proton, nitrogen, and carbonyl chemical shielding anisotropies in a protein dissolved in a dilute liquid crystalline phase. J Am Chem Soc 122:10143–10154

Cornilescu G, Delaglio F, Bax A (1999) Protein backbone angle restraints from searching a database for chemical shift and sequence homology. J Biomol NMR 13:289–302

Cossi M, Scalmani G, Rega N, Barone V (2002) New developments in the polarizable continuum model for quantum mechanical and classical calculations on molecules in solution. J Chem Phys 117:43–54

Damberg P, Jarvet J, Graslund A (2005) Limited variations in 15N CSA magnitudes and orientations in ubiquitin are revealed by joint analysis of longitudinal and transverse NMR relaxation. J Am Chem Soc 127:1995–2005

De Dios AC, Pearson JG, Oldfield E (1993) Secondary and tertiary structural effects on protein NMR chemical-shifts–an ab initio approach. Science 260:1491–1496

Dellwo MJ, Wand AJ (1989) Model-independent and model-dependent analysis of the global and internal dynamics of cyclosporine-A. J Am Chem Soc 111:4571–4578

Dunning TH (1989) Gaussian-basis sets for the use in correlated molecular calculations. 1. The atomic boron through neon and hydrogen. J Chem Phys 90:1007–1023

Elavarasi SB, Dorai K (2010) Mapping NMR chemical shift anisotropy parameters of backbone nuclei onto secondary structure elements in proteins. J Biomol Struct Dyn 27:561–572

Feller D (1996) The role of databases in support of computational chemistry calculations. J Comput Chem 17:1571–1586

Francl MM, Pietro WJ, Hehre WJ, Binkley JS, Gordon MS, Defrees DJ, Pople A (1982) Self-consistent molecular-orbital methods. 23. A polarization-type basis set for 2nd-row elements. J Chem Phys 77:3654–3665

Frisch MJTGW, Schlegel HB, Scuseria GE, Robb MA, Cheeseman JR, Scalmani G, Barone V, Mennucci B, Petersson GA, Nakatsuji H, Caricato M, Li X, Hratchian HP, Izmaylov AF, Bloino J, Zheng G, Sonnenberg JL, Hada M, Ehara M, Toyota K, Fukuda R, Hasegawa J, Ishida M, Nakajima T, Honda Y, Kitao O, Nakai H, Vreven T, Montgomery Jr JA, Peralta JE, Ogliaro F, Bearpark M, Heyd JJ, Brothers E, Kudin KN, Staroverov VN, Kobayashi R, Normand J, Raghavachari K, Rendell A, Burant JC, Iyengar SS, Tomasi J, Cossi M, Rega N, Millam JM, Klene M, Knox JE, Cross JB, Bakken V, Adamo C, Jaramillo J, Gomperts R, Stratmann RE, Yazyev O, Austin, AJ, Cammi R, Pomelli C, Ochterski JW, Martin RL, Morokuma K, Zakrzewski VG, Voth GA, Salvador P, Dannenberg JJ, Dapprich S, Daniels AD, Farkas Ö, Foresman JB, Ortiz JV, Cioslowski J, Fox DJ (2009) Gaussian, Inc., Wallingford

Fushman D, Cowburn D (1998) Model-independent analysis of N-15 chemical shift anisotropy from NMR relaxation data. Ubiquitin as a test example. J Am Chem Soc 120:7109–7110

Fushman D, Cowburn D (1999) The effect of noncollinearity of 15N-1H dipolar and 15N CSA tensors and rotational anisotropy on 15N relaxation, CSA/dipolar cross correlation, and TROSY. J Biomol NMR 13:139–147

Fushman D, Cowburn D (2001) Nuclear magnetic resonance relaxation in determination of residue-specific 15N chemical shift tensors in proteins in solution: protein dynamics, structure, and applications of transverse relaxation optimized spectroscopy. Methods Enzym 339:109–126

Fushman D, Tjandra N, Cowburn D (1998) Direct measurement of N-15 chemical shift anisotropy in solution. J Am Chem Soc 120:10947–10952

Gardino AK, Villali J, Kivenson A, Lei M, Liu CF, Steindel P, Eisenmesser EZ, Labeikovsky W, Wolf-Watz M, Clarkson MW, Kern D (2009) Transient non-native hydrogen bonds promote activation of a signaling protein. Cell 139:1109–1118

Hall JB, Fushman D (2006) Variability of the 15N chemical shielding tensors in the B3 domain of protein G from 15N relaxation measurements at several fields. Implications for backbone order parameters. J Am Chem Soc 128:7855–7870

Hariharan PC, Pople A (1973) Influence of polarization functions on molecular-orbital hydrogenation energies. Theor Chim Acta 28:213–222

Harris RK, Becker ED, De Menezes SM, Granger P, Hoffman RE, Zilm KW (2008) Further conventions for NMR shielding and chemical shifts (IUPAC Recommendations 2008). Magn Reson Chem 46:582–598

Hehre WJ, Ditchfield R, Pople A (1972) Self-consistent molecular-orbital methods. 12. Further extensions of gaussian-type basis sets for use in molecular-orbital studies of organic molecules. J Chem Phys 56:2257

Helgaker T, Jaszunski M, Ruud K (1999) Ab initio methods for the calculation of NMR shielding and indirect spin–spin coupling constants. Chem Rev 99:293–352

Hiyama Y, Niu CH, Silverton JV, Bavoso A, Torchia DA (1988) Determination of N-15 chemical-shift tensor via N-15-H-2 dipolar coupling in boc-glycylglycyl[N-15]glycine benzyl ester. J Am Chem Soc 110:2378–2383

Hubbard MJ, Cohen P (1993) On target with a new mechanism for the regulation of protein phosphorylation. Trends Biochem Sci 18:172–177

Jensen F (2008) Basis set convergence of nuclear magnetic shielding constants calculated by density functional methods. J Chem Theory Comput 4:719–727

Jiménez JL, Hegemann B, Hutchins JRA, Peters JM, Durbin R (2007) A systematic comparative and structural analysis of protein phosphorylation sites based on the mtcPTM database. Genome Biol 8:R90

Johnson LN, Lewis RJ (2001) Structural basis for control by phosphorylation. Chem Rev 101:2209–2242

Kay LE, Torchia DA, Bax A (1989) Backobone dynamics of proteins as studied by N-15 inverse detected heteronuclear NMR-spectroscopy–application to staphylococcal nuclease. Biochemistry 28:8972–8979

Krishnan R, Binkley JS, Seeger R, Pople A (1980) Self-consistent molecular-orbital methods. 20. Basis set for correlated wave-functions. J Chem Phys 72:650–654

Kroenke CD, Rance M, Palmer AG (1999) Variability of the N-15 chemical shift anisotropy in *Escherichia coli* ribonuclease H in solution. J Am Chem Soc 121:10119–10125

Kurita J, Shimahara H, Utsunomiya-Tate N, Tate S (2003) Measurement of 15N chemical shift anisotropy in a protein dissolved in a dilute liquid crystalline medium with the application of magic angle sample spinning. J Magn Reson 163:163–173

Kutzelnigg W, Fleischer U, Schindler M (1990) NMR, basic principles and progress. Springer, Heidelberg

Lancelot N, Elbayed K, Piotto M (2005) Applications of variable-angle sample spinning experiments to the measurement of scaled residual dipolar couplings and (15)N CSA in soluble proteins. J Biomol NMR 33:153–161

Landrieu I, Lacosse L, Leroy A, Wieruszeski JM, Trivelli X, Sillen A, Sibille N, Schwalbe H, Saxena K, Langer T, Lippens G (2006) NMR analysis of a Tau phosphorylation pattern. J Am Chem Soc 128:3575–3583

Le HB, Oldfield E (1996) Ab initio studies of amide-N-15 chemical shifts in dipeptides: applications to protein NMR spectroscopy. J Phys Chem 100:16423–16428

Lee DK, Wittebort RJ, Ramamoorthy A (1998) Characterization of N-15 chemical shift and H-1-N-15 dipolar coupling interactions in a peptide bond of uniaxially oriented and polycrystalline samples by one-dimensional dipolar chemical shift solid-state NMR spectroscopy. J Am Chem Soc 120:8868–8874

Lee DK, Wei Y, Ramamoorthy A (2001) A two-dimensional magic-angle decoupling and magic-angle turning solid-state NMR method: an application to study chemical shift tensors from peptides that are nonselectively labeled with 15N isotope. J Phys Chem B 105:4752–4762

Liokatis S, Dose A, Schwarzer D, Selenko P (2010) Simultaneous detection of protein phosphorylation and acetylation by high-resolution NMR spectroscopy. J Am Chem Soc 132:14704–14705

Liokatis S, Stützer A, Elsässer SJ, Theillet FX, Klingberg R, van Rossum B, Schwarzer D, Allis CD, Fischle W, Selenko P (2012) Phosphorylation of histone H3 Ser10 establishes a hierarchy for subsequent intramolecular modification events. Nat Struct Mol Biol 19:819–823

Lipari G, Szabo A (1982a) Model-free approach to the interpretation of nuclear magnetic-resonance relaxation in macromolecules. 1. Theory and range of validity. J Am Chem Soc 104:4546–4559

Lipari G, Szabo A (1982b) Model-free approach to the interpretation of nuclear magnetic-resonance relaxation in macromolecules.2. Analysis of experimental results. J Am Chem Soc 104:4559–4570

Lipsitz RS, Tjandra N (2003) 15N chemical shift anisotropy in protein structure refinement and comparison with NH residual dipolar couplings. J Magn Reson 164:171–176

Lumsden MD, Wu G, Wasylishen RE, Curtis RD (1993) Solid-state N-15 NMR-studies of the nitroso group in the nitrobenzene dimmer and p-nitroso-N, N-dimethyllaniline. J Am Chem Soc 115:2825–2832

Markley JL, Bax A, Arata Y, Hilbers CW, Kaptein R, Sykes BD, Wright PE, Wuthrich K (1998) Recommendations for the presentation of NMR structures of proteins and nucleic acids. IUPAC-IUBMB-IUPAB Inter-Union Task Group on the standardization of data bases of protein and nucleic acid structures determined by NMR spectroscopy. J Biomol NMR 12:1–23

Mason AJ, Grage SL, Straus SK, Glaubitz C, Watts A (2004) Identifying anisotropic constraints in multiply labeled bacteriorhodopsin by N-15 MAOSS NMR: a general approach to structural studies of membrane proteins. Biophys J 86:1610–1617

McLean AD, Chandler GS (1980) Contracted gaussian-basis sets for molecular calculations. 1. 2nd row atoms, Z-11–18. J Chem Phys 72:5639–5648

Metcalfe EE, Traaseth NJ, Veglia G (2005) Serine 16 phosphorylation induces an order-to-disorder transition in monomeric phospholamban. Biochemistry 44:4386–4396

Neal S, Berjanskii M, Zhang HY, Wishart DS (2006) Accurate prediction of protein torsion angles using chemical shifts and sequence homology. Mag Reson Chem 44:S158–S167

Otten R, Villali J, Kern D, Mulder FA (2010) Probing microsecond time scale dynamics in proteins by methyl (1)H Carr-Purcell-Meiboom-Gill relaxation dispersion NMR measurements. Application to activation of the signaling protein NtrC(r). J Am Chem Soc 132:17004–17014

Pandey MK, Vivekanandan S, Ahuja S, Pichumani K, Im SC, Waskell L, Ramamoorthy A (2012) Determination of 15N chemical shift anisotropy from a membrane-bound protein by NMR spectroscopy. J Phys Chem B 116:7181–7189

Pawson T, Scott JD (2005) Protein phosphorylation in signaling—50 years and counting. Trends Biochem Sci 30:286–290

Peng JW, Wagner G (1992) Mapping of the spectral densities of N-H bond motions in eglin c using heteronuclear relaxation experiments. Biochemistry 31:8571–8586

Pervushin K, Riek R, Wider G, Wuthrich K (1997) Attenuated T2 relaxation by mutual cancellation of dipole–dipole coupling and chemical shift anisotropy indicates an avenue to NMR structures

of very large biological macromolecules in solution. Proc Natl Acad Sci USA 94:12366–12371

Poon A, Birn J, Ramamoorthy A (2004) How does an amide-15N chemical shift tensor vary in peptides? J Phys Chem B 108: 16577–16585

Saitôa H, Andob I, Ramamoorthy A (2010) Chemical shift tensor—the heart of NMR: insights into biological aspects of proteins. Prog Nucl Magn Reson Spectrosc 57:181–228

Schuchardt KL, Didier BT, Elsethagen T, Sun LS, Gunrumoorthi V, Chase J, Li J, Windus TL (2007) Basis set exchange: a community database for computational sciences. J Chem Inf Model 47:1045–1052

Shen Y, Bax A (2007) Protein backbone chemical shifts predicted from searching a database for torsion angle and sequence homology. J Biomol NMR 38:289–302

Shen Y, Delaglio F, Cornilescu G, Bax A (2009) TALOS plus: a hybrid method for predicting protein backbone torsion angles from NMR chemical shifts. J Biomol NMR 44:213–223

Sychrovský V, Buděšínský M, Benda L, Špirko V, Vokacova Z, Šebestík J, Bouř P (2008) Dependence of the L-alanyl-L-alanine conformation on molecular charge determined from ab initio computations and NMR spectra. J Phys Chem 112:1796–1805

Tang S, Case DA (2007) Vibrational averaging of chemical shift anisotropies in model peptides. J Biomol NMR 38:255–266

Tang S, Case DA (2011) Calculation of chemical shift anisotropy in proteins. J Biomol NMR 51:303–312

Volkman BF, Lipson D, Wemmer DE, Kern D (2001) Two-state allosteric behavior in a single-domain signaling protein. Science 291:2429–2433

Waddell KW, Chekmenev EY, Wittebort RJ (2005) Single-crystal studies of peptide prolyl and glycyl N-15 shielding tensors. J Am Chem Soc 127:9030–9035

Wang B, Fleischer U, Hinton JF, Pulay P (2001) Accurate prediction of proton chemical shifts. I. Substituted aromatic hydrocarbons. J Comput Chem 22:1887–1895

Wang B, Hinton JF, Pulay P (2002) Accurate prediction of proton chemical shifts. II. Peptide analogues. J Comp Chem 23:492–497

Wolinski K, Hinton JF, Pulay P (1990) Efficient implementation of the gauge-independent atomic orbital method for NMR chemical-shift calculations. J Am Chem Soc 112:8251–8260

Woon DE, Dunning TH (1993) Gaussian-basis sets for use in correlated molecular calculations. 3. The atoms aluminium through argon. J Chem Phys 98:1358–1371

Wylie BJ, Franks WT, Graesser DT, Rienstra CM (2005) Site-specific 13C chemical shift anisotropy measurements in a uniformly 15N, 13C-labeled microcrystalline protein by 3D magic-angle spinning NMR spectroscopy. J Am Chem Soc 127:11946–11947

Wylie BJ, Franks WT, Rienstra CM (2006) Determinations of 15N chemical shift anisotropy magnitudes in a uniformly 15N, 13C-labeled microcrystalline protein by three-dimensional magic-angle spinning nuclear magnetic resonance spectroscopy. J Phys Chem 110:10926–10936

Wylie BJ, Sperling LJ, Frericks HL, Shah GJ, Franks WT, Rienstra CM (2007) Chemical-shift anisotropy measurements of amide and carbonyl resonances in a microcrystalline protein with slow magic-angle spinning NMR spectroscopy. J Am Chem Soc 129:5318–5319

Xu XP, Case DA (2002) Probing multiple effects on 15N, 13C alpha, 13C beta, and 13C' chemical shifts in peptides using density functional theory. Biopolymers 65:408–423

Yao L, Grishaev A, Cornilescu G, Bax A (2010) Site-specific backbone amide (15)N chemical shift anisotropy tensors in a small protein from liquid crystal and cross-correlated relaxation measurements. J Am Chem Soc 132:4295–4309

Zuiderweg ER (2002) Mapping protein–protein interactions in solution by NMR spectroscopy. Biochemistry 41:1–7